CA II LINES IN A QUIET REGION ON THE SUN
I. DYNAMIC PROCESSES IN THE SOLAR ATMOSPHERE

I.P. Turova
Institute of Solar-Terrestrial Physics SB RAS
Irkutsk, Russia, turova@iszf.irk.ru

S.A. Grigoryeva
Institute of Solar-Terrestrial Physics SB RAS
Irkutsk, Russia, sgrig@iszf.irk.ru

O.A. Ozhogina
Institute of Solar-Terrestrial Physics SB RAS
Irkutsk, Russia, ozhog@iszf.irk.ru

Abstract. We have studied oscillation processes in the quiet Sun outside a coronal hole at different levels of the solar chromosphere. The study was based on spectroscopic observations of ionized calcium lines (K, H, and 849.8 nm) obtained by the Sayan Solar Observatory's Automated Solar Telescope (AST). Spectral analysis of time series for some parameters of the lines has been carried out. We have compared the results of this work with the results of our study of oscillation processes in quiet regions located at the base of a coronal hole. The oscillation power was found to be higher in the region of the quiet Sun outside a coronal hole. At the same time, for the regions under study there is a common tendency for the oscillation power to decrease with height for all frequency ranges, except for the low-frequency one, in most chromospheric structures. In structures with a weak magnetic field, the power increases with height to the lower chromosphere and decreases somewhat to the upper chromosphere.

Keywords: chromosphere, Ca II line profiles, oscillation processes.

INTRODUCTION

The upper solar atmosphere heating is one of the key problems in solar physics. Of particular importance in this context is the solar chromosphere [Athay, 1966; Goodman, 2000; Carlsson, 2006; Judge, 2009; Srivastava et al., 2021]. It serves as an interface between the relatively cold photosphere and the very hot corona [Judge, 2010; Jess et al., 2015] and is a region in which a significant part of dissipative processes occur.

The processes occurring in the chromosphere are determined by its thermodynamic conditions. This is an environment in which there is non-local thermodynamic equilibrium; ionization equilibrium is disturbed; radiative losses occur, their velocity is $4 \cdot 10^6$ erg·cm^{-2}·s^{-1} in a quiet region (for comparison, in the corona this value is $3 \cdot 10^5$ erg·cm^{-2}·s^{-1}) (see Table 1 in [Withbroe, Noyes, 1977]). It is permeated with dynamic structures, magnetic fields and is extremely stratified [Judge, 2009]. For instance, for the 1D model VAL C [Vernazza et al., 1981] at a height range from a temperature minimum to ≈2 Mm, pressure changes by four orders of magnitude. Chromospheric magnetic fields affect wave propagation, conversion, and dissipation.

Under the temperature regime that takes place in the chromosphere, its material consists of partially ionized plasma dominated by neutrals. Thus, the VAL C model [Vernazza et al., 1981] in the region of temperature minimum yields a degree of hydrogen ionization of 10^{-4}, which increases toward the middle chromosphere up to ~10^{-3}–10^{-2} at temperatures ~6000 K.

The presence of neutrals in partially ionized magnetized plasma influences the processes that cause the upper atmosphere to heat [Piddington, 1956; Cowling, 1956; Khomenko, Collados, 2012; Martinez-Sikora et al., 2015 and references therein]. A realistic approach to modeling the processes occurring in the chromosphere is based on principles of plasma physics. Representation of a multifluid (multicomponent) medium is used. Depending on the problem to solve, the plasma composition can be three-component (electrons, ions, and neutral atoms), two-component (ions and neutrals), as well as one-component (with a strong connection between electrons, ions and neutral atoms) (e.g., [Zaqarashvili et al., 2011; Khomenko, Collados, 2012; Ballester et al., 2020]). The results of such simulation show, in particular, that the presence of neutral atoms in a weakly ionized plasma increases the dissipation of MHD waves [Khodachenko et al., 2004], and also changes the rate of reconnection depending on the collisional coupling between ions and neutrals [Zweibel, 1989; Smith, Sakai, 2008].

Our knowledge of the solar atmosphere has extended significantly thanks to the development of theoretical foundation and the progress in computational tools. Nonetheless, the problem of heating the solar atmosphere is still relevant today.

To date, two main theories have been formed concerning the mechanisms of upper atmosphere heating (see, e.g., [Rajaguru et al., 2019] and references therein): 1) mechanical heating by waves of various types such as nonmagnetic waves, magnetic waves, and their combination; 2) magnetic energy dissipation due to various processes in the magnetic field.

A large number of works have been carried out on various sources of chromosphere and corona heating (e.g., [Jefferies et al., 2006; Shibata et al., 2007; Kayshap et al., 2018; Leenaarts et al., 2018]). Reviews have been written which summarize and analyze recent re-

sults ([Khomenko, Santamaria, 2013; Jess et al., 2015; Martinez-Sikora et al., 2015; Ballester et al., 2018; Srivastava et al., 2021] and references therein).

In terms of solar atmosphere heating, of particular importance is the question of the role of MHD waves in energy transfer from the photosphere to the chromosphere and corona. There are still many unresolved problems related to the possibilities of compensating for radiative losses in the chromosphere, transition region, and corona by wave processes. For example, Molnar et al. [2021] have presented observations and comparison with the model, which concern propagation and damping of acoustic waves with frequencies from 5 to 50 mHz in different chromospheric structures: internetwork, network, plages, and penumbra. Their findings show that the acoustic energy dissipation in the middle chromosphere is not the dominant heating mechanism, whereas in the internetwork of the upper chromosphere the contribution of acoustic waves can compensate for radiative losses. The data obtained by Abbasvand et al. [2020], on the other hand, suggests that in the middle chromosphere of the quiet Sun radiative losses are fully balanced by the deposited acoustic energy flux in the range ~1–8 mHz.

In this paper, we examine dynamic processes using the Ca II H and K lines, and the 849.8 nm infrared triplet line, which are a convenient tool for studying the solar atmosphere. The Ca II lines are formed in a wide range of heights, from the lower to the middle and upper chromosphere. Thus, according to the results of 3D modeling [Bjørgen et al., 2018], cores of the K and H lines are formed at altitudes of ≈1900 km and 1750 km. For the 849.8 nm line, the results of 2D modeling [Pietarila et al., 2006] give an average altitude of ≈1020 km.

The purpose of this work is to study oscillatory processes at different height levels of the chromosphere in a quiet region outside a coronal hole and compare these results with the results for quiet regions at the base of the coronal hole.

1. OBSERVATIONS AND THEIR PROCESSING

We observed a quiet region with coordinates N05W00 located outside a coronal hole. The observations were made with the Sayan Solar Observatory's Horizontal Solar Telescope on June 12, 2006. Two spectral regions in ultraviolet and infrared bands were recorded simultaneously in the IV and II orders respectively. We used the Princeton Instruments 2048×2048 CCD camera with a spatial pixel size of 0".45. The region on the Sun bounded by the spectrograph slit was about 200" (450 pixels). The time series had 40 frames with a time step of 25 s. An image of a part of the solar disk including the observed region is shown in Figure 1 (data from the open source [https://SolarMonitor.org]). The black line superimposed on the image indicates the position of the spectrograph slit, taking into account its shift at the beginning of observations.

The research subject of our paper is intensities at characteristic points of the K, H, and 849.8 nm line profiles, as well as shifts of the profiles at these points along the wavelength.
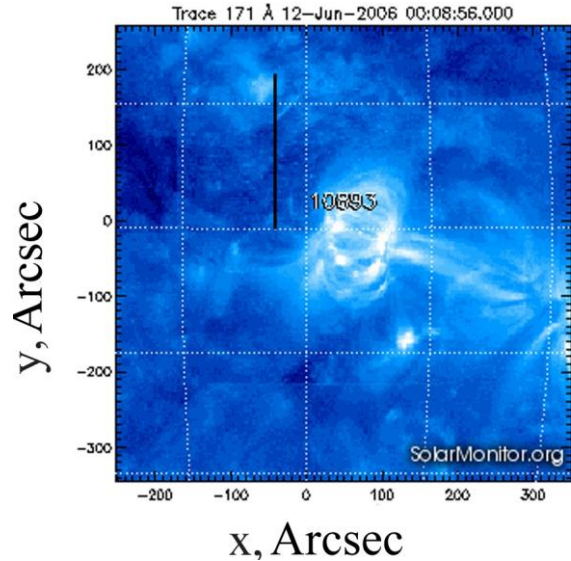

Figure 1. Image of a part of the solar disk on June 12, 2006, taken from an open source. The black stripe is the spectrograph slit with a shift at the beginning of observations

We designate the 849.8 nm line by X (as in [Shine, Linsky, 1974]).

The following quantitative parameters have been determined:

- I_{K3}, I_{H3} — minimum central intensities of the K and H lines;
- I_{K2v}, I_{K2r}, I_{H2v}, I_{H2r} — intensities of the violet and red emission peaks respectively;
- I_{K1v}, I_{K1r}, I_{H1v}, I_{H1r} — minimum intensities in the violet and red wings of the K and H lines respectively;
- I_{X0} — central intensity of the 849.8 nm line;
- λ_{K3} — shift of the K_3 minimum along the wavelength axis relative to the nominal line center;
- $\Delta\lambda_{K2v}$, $\Delta\lambda_{K2r}$ — shifts of the K_{2v} and K_{2r} peaks relative to the nominal line center;
- $\Delta\lambda_{X0}$ — shift of the 849.8 nm line minimum along the wavelength axis relative to the nominal line center;
- $\Delta\lambda_{K1v}$, $\Delta\lambda_{K1r}$ — shifts of K_{1v} and K_{1r} minima relative to the nominal line center.

As noted earlier in [Teplitskaya et al., 2006; Grigoryeva, et al., 2016; Teplitskaya et al., 2009; Turova et al., 2020], we selected the chromospheric structures according to central intensities of the Ca II K and 849.8 nm lines. The structures are defined as in the above works:

- "n" — bright network structures («network»);
- "ne" — enhanced network;
- "c" — dark internetwork structures («internetwork»);
- "b" — plage;
- "x" — structures with intermediate brightness, which do not belong to the above structures.

In addition to the above list, this paper also deals with structures whose intensities are close to the intensities on the boundaries of each of the above structures. By analogy with the designations we have adopted, these regions are called "fc", "fx", "fn", "fne", "fb".
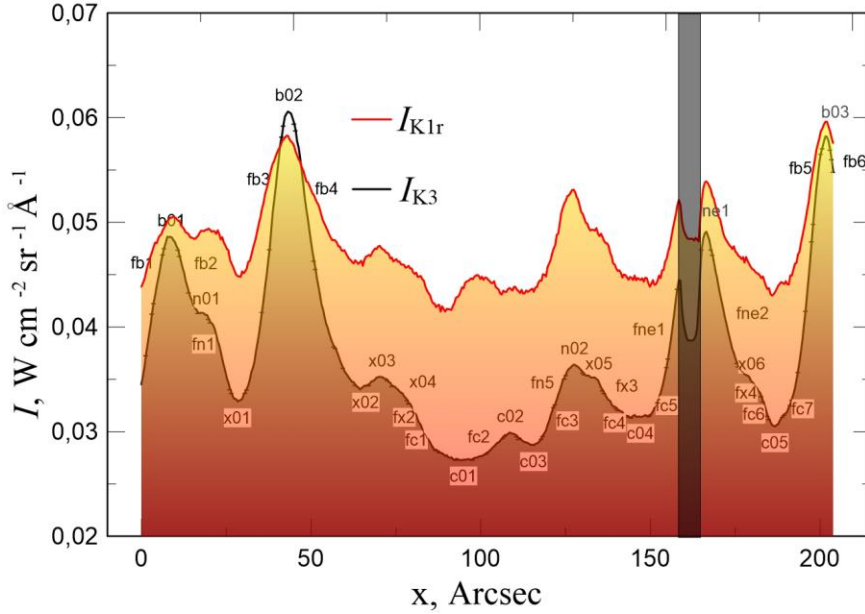
Figure 2. Intensities I_{K3} (black curve) and I_{K1r} (red curve) for the spatial region N05W00 along the spectrograph slit, which are averaged over the observation time. Alphanumeric designations mark some of the selected chromospheric structures. The black vertical stripe is a thread stretched across the spectrograph slit

Figure 2 shows time-averaged spatial distributions of I_{K3} and $I_{K1r.}$ The alphanumeric designations describe some of the selected structures. The behavior of both intensities shows slight spatial differences in positions of the structures at the I_{K3} and I_{K1r} formation levels, which may be caused by atmospheric dispersion. Atmospheric dispersion effects have been examined in a number of papers, for example, [Simon, 1966; Reardon, 2006; Beck et al., 2008]. Atmospheric dispersion results from two processes: a change in atmospheric refraction with zenith distance, known as spatial differential refraction; a change in the air refraction index with wavelength, called spectral differential refraction [Reardon, 2006]. In order to avoid mathematical determination of locations of different spatial elements at different levels of the atmosphere, we determined locations of the structures separately for each of these levels.

In this paper, we examine spatial and temporal variations of lines' parameters in the selected structures. We estimate the oscillation power at different levels of the solar atmosphere. Spectral analysis of the lines' parameters is performed at each point of space of the region under study. A method is adopted similar to that used in [Grigoryeva et al., 1916; Kopetsky, Kuklin, 1971; Turova et al., 1983, Teplitskaya et al., 1983; Turova, 1994]. The following frequency bands are selected:

- 5.2–6.8 mHz (3 min);
- 5.2–8.0 mHz (sometimes used in the literature as a 3-min band);
- 4.0–5.2 (4 min);
- 2.4–4.0 (5 min);
- 2.4–5.2 (5 min+4 min);
- 2.4–8.0 (5 min+4 min+3 min);
- 1.124–2.4 (low frequencies, "L");
- 8.0–16.0 (high frequencies, "H");
- 1.124–16.0 (full frequency band available, "E").

Using the spectral analysis results, we focus on the study of distributions of the integrated spectral power of intensity oscillations and line profile shifts in different frequency bands both throughout the region of interest and in individual chromospheric structures.

2.   RESULTS

2.1. Spatio-temporal variations in lines' parameters

Figure 3 displays spatial and temporal distributions of a number of line parameters. For this figure, we took I_{K1v}, abs($\Delta\lambda_{K1v}$), I_{X0}, $\Delta\lambda_{X0}$, I_{K2v}, abs($\Delta\lambda_{K2v}$), I_{K3}, ($-\Delta\lambda_{K3}$), which illustrate the characteristic features of the behavior of parameters of this type. The values of $\Delta\lambda_{K3}$ are given with a minus sign for perception convenience because for the absolute majority of points the CaII K line minimum is shifted to the violet side. Figure 4 exhibits time-averaged spatial distributions of abs($\Delta\lambda_{K1v}$), abs($\Delta\lambda_{K2v}$), abs($\Delta\lambda_{K3}$), as well as the spatial distribution of the integrated spectral power (ISP) for shifts in one of the frequency bands. To compare the distributions of $\Delta\lambda_K$ with the spatial distribution of chromospheric structures, each panel of Figure 4 also shows the spatial distribution of the time-averaged intensity I_{K3}.

The behavior of profile shifts (see Figure 3) differs significantly in space from the behavior of intensities: shift distributions are more chaotic than intensity distributions. The comparison indicates that at the K_1 formation level the $\Delta\lambda_{K1}$ variation correlates more closely with the intensity variation than at the K_2 and K_3 levels. At the K_1 level, to the intensity peaks in bright magnetic structures correspond high values of $\Delta\lambda_{K1}$ (Figure 4, *a*). Shifts at the K_2 level are increased at boundaries of magnetic structures, not in their central parts. This is confirmed by Figure 4, *b*, which illustrates time- averaged

spatial distributions of abs($\Delta\lambda_{K2v}$). The scatter plots for the pairs of parameters $\Delta\lambda_{K1}$–I_{K1}, $\Delta\lambda_{K2}$–I_{K2} in Figure 5, *e, g* in [Turova et al., 2020] also suggest the connection between parameters at the K_1 level and its absence at the K_2 level. At the highest level K_3 under study, shifts are also increased at boundaries of bright magnetic structures, but the largest shifts occur in the most quiet non-magnetic structures of the observed region (from 70″ to 140″ along the X-axis (Figure 4,*c*)). The main oscillatory power of $\Delta\lambda_{K3}$ for quiet structures has been found in the range 4–8 mHz. Five-minute oscillations in this region are negligible, but decreased oscillations of $\Delta\lambda_{K3}$ were detected in the low frequency range (not shown). Interestingly, the highest power peaks at frequencies around 5.5 and 7 mHz were found for the "c02" structure, yet the velocity amplitudes in it exhibited a significant decrease (see Figure 4, *c*). The "c02" structure shows an increase in brightness as compared to neighboring structures of this type. Note that spatial distributions of the integrated spectral power of oscillations of $\Delta\lambda_{K1v}$, $\Delta\lambda_{K2v}$, and $\Delta\lambda_{K3}$ are complex and multiple-peaked. The spatial distribution of maximum power peaks in a given frequency band may not match the spatial distribution of maximum shifts $\Delta\lambda_K$. Therefore, in Figure 4 for each of the above parameters we took the frequency band in which the correspondence of maximum shifts and power peaks in space was the closest.

In order to estimate the degree of relationship between shifts $\Delta\lambda_K$ and their related values of I_K, as well as the ISP($\Delta\lambda_K$) values shown in Figure 4, we calculated correlation coefficients. They are listed in Table 1. Rows 1–3 show the correlation between $\Delta\lambda_K$ and intensities. Rows 4–6 display the integrated spectral power, with ISP correlations both for the entire region of interest and for half of the region from 0″ to 100″. In the third column for rows 4–6 is the frequency band for which the maximum correlation coefficient was found.

Table 1 allows us to quantitatively estimate the qualitative pattern presented in Figures 3, 4. So, at the K_1 level (Figure 4, *a*), where maximum shifts $\Delta\lambda_{K1v}$ coincide with the I_{K1} peaks, the correlation coefficient of the time-averaged parameters $\Delta\lambda_{K1v}$ and I_{K1} in the region under study is >0.9.

The correlation coefficient of $\Delta\lambda_{K1v}$ with ISP($\Delta\lambda_{K1v}$) in the 5-minute band for half (0″–100″) of the region under study is 0.7. For the entire region of interest, it is significantly lower, ~0.3.

As mentioned above, the maximum shifts $\Delta\lambda_{K2v}$ at the K_2 level often occur not in the centers of magnetic structures (Figure 4, *b*). On the contrary, in the centers of magnetic structures the shifts decrease (see, for example, their values in plage "b02": position on the X-axis ≈50″). The correlation coefficient between $\Delta\lambda_{K2v}$ and I_{K2v} is ≈0.1 (Table 1, row 2).

At the K_3 level, as can be seen in Figure 4, *c*, the largest shifts $\Delta\lambda_{K3}$ fall on the quietest part of the region under study. The shifts, as at the K_2 level, are insignificant in the centers of magnetic structures. The correlation coefficient between $\Delta\lambda_{K3}$ and I_{K3} is ≈0.2 (row 3, Table 1). The correlation coefficient between $\Delta\lambda_{K3}$ and the integrated spectral power of oscillations of this parameter in the 5-minute band over the entire region considered is 0.2, yet it can reach 0.5 for individual structures of the region (Table 1, row 6).

Obviously, oscillations of different frequencies can dominate in different structures. To explore this problem in more detail, we have selected several characteristic features of the region under study. At the K_1 level there are two features the former of which corresponds to "b02". Here, the maximum shifts $\Delta\lambda_{K1v}$ and $\Delta\lambda_{K1r}$ fall on the center of the plage. The latter feature was chosen in a quiet region — in "c01". At the K_2 level, these are two features in the vicinity of the plage with maximum shifts $\Delta\lambda_{K2v}$ and the structure "c01". At the K_3 level, this is a feature in the vicinity of "b02" and the structure "c01". For these features, we have found correlation coefficients between $\Delta\lambda_{K1v}$, $\Delta\lambda_{K2v}$, $\Delta\lambda_{K3}$ and the oscillation power P at each point of the frequency band 1.1–16.0 mHz. Maximum correlation coefficients between P and shifts for these structures, as well as the frequency for which the oscillation power is maximum, are given in rows 7–9 of Table 1. It turned out that in the selected features the local oscillation maxima obtained have not very high correlation coefficients with $\Delta\lambda_K$ ($r\sim$0.5–0.6). The highest correlation coefficient (0.75) was found for the feature near «b02» at the K_3 level.

2.2. Integrated spectral power of intensity oscillations at different levels of the solar atmosphere

2.2.1. Variation of integrated spectral power with height

We have compared the integrated spectral power of intensity oscillations at different levels of the solar atmosphere, using the height of different spectral features of the K, H, 849.8 nm lines as markers. These are I_{H1r}, I_{K1r}, I_{H1v}, I_{K1v}, I_{H2r}, I_{K2r}, I_{X0}, I_{H2v}, I_{K2v}, I_{H3}, I_{K3}, ranked according to the data on heights of their formation available in the literature [von Uexküll, Kneer, 1995; Taroyan, Erdélyi, 2009; Judge et al., 2001; Reardon et al., 2009; Beck et al., 2009; Bjørgen, et al., 2018]. We plotted Figure 5, *a–f* similar to Figure 13 from [Grigoryeva et al., 2016]. In this paper, we use a slightly different set of height markers and a larger number of frequency bands. As an example, Figure 5 shows the behavior of the spatially averaged integrated spectral power of intensity oscillations for individual structures and for the whole observed region in the selected frequency bands.

In the entire frequency band (1.124–16.0 mHz), the oscillation power turned out to decrease with height in the solar atmosphere in each individual structure and throughout the area cut out by the spectrograph slit (Figure 5). An exception is the structure "c" in which there is a slight increase in the oscillation power in the entire frequency band (Figure 5, *a*). This structure and the "fc" structure (Figure 5, *b*) are also distinguished by an increase in 3-minute oscillations with height. The "c" structure also exhibits a slight increase in high-frequency oscillations (8–16 mHz) and a slight decrease in the power of low-frequency oscillations (1.124–2.4 mHz, Figure 5, *a*). In "fc", on the contrary, high-frequency oscillations decrease with height, and low-frequency oscillations increase (Figure 5, *b*).
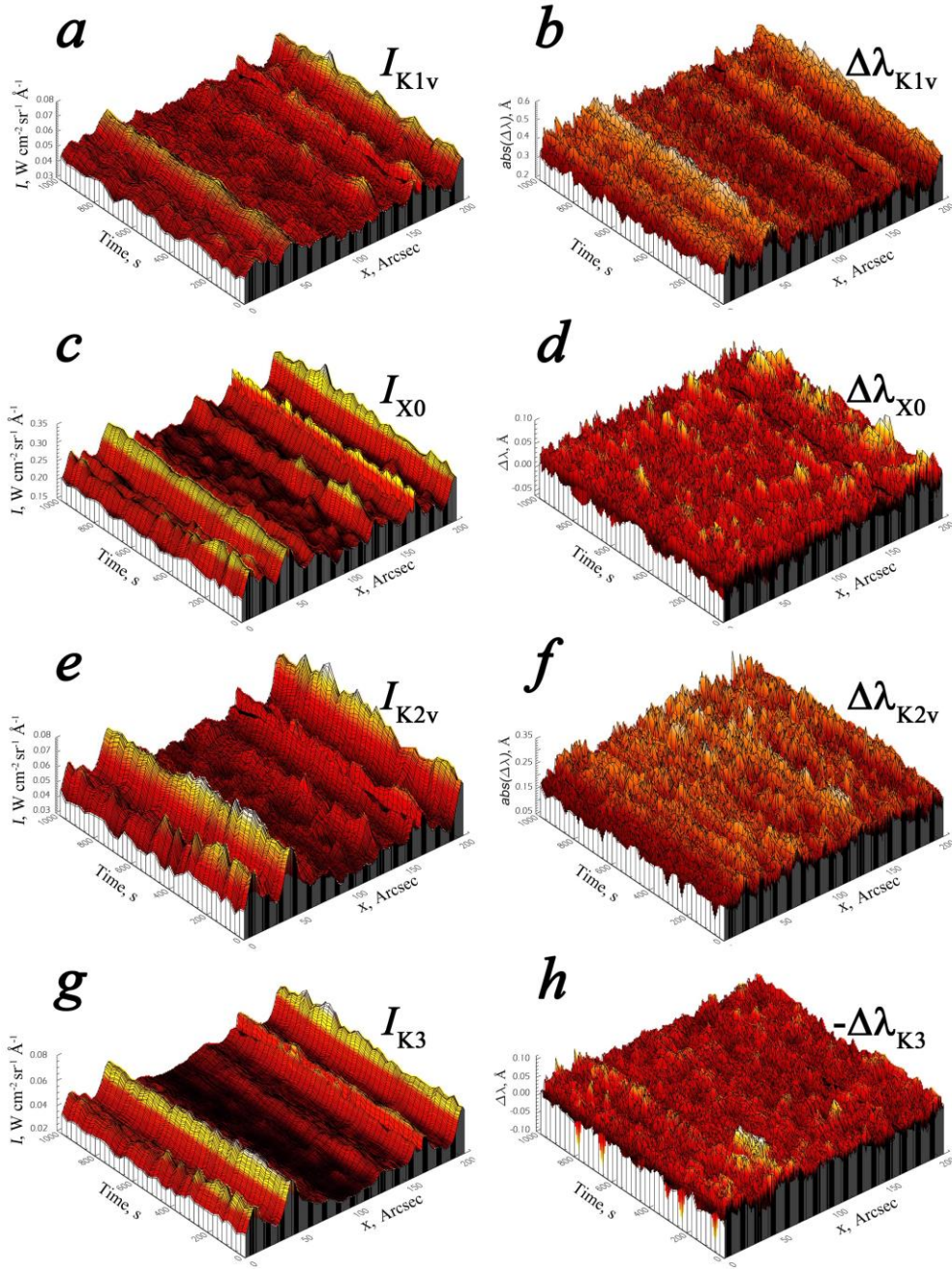
Figure 3. Spatial-temporal distributions of some parameters of the CaII K and 849.8 nm lines: intensity I_{K1v} (*a*); shift abs($\Delta\lambda_{K1v}$) (*b*); intensity I_{X0} (*c*); shift $\Delta\lambda_{X0}$ (*d*); intensity I_{K2v} (*e*); shift abs($\Delta\lambda_{K2v}$) (*f*); intensity I_{K3} (*g*); shift ($-\Delta\lambda_{K3}$) (*h*). Along the axes are the time of observations of the series, the spatial coordinate (along the spectrograph slit), and parameter values. Line shifts are in angstroms

The remaining structures, including those not shown in Figure 5, exhibit a decrease in the oscillation power in all frequency bands except for low-frequency and high-frequency ones. The same behavior is also typical of the whole region on the Sun under study, including all the selected structures, as well as structures not included in the classification (Figure 5, *d*). Exceptions are the enhanced network with a pronounced slight increase in the power of 5-minute oscillations (Figure 5, *e*), and the "fx" boundary (Figure 5, *f*) in which the behavior of 3-minute and high-frequency oscillations does not show a confident tendency for the oscillation power to decrease or increase.

2.2.2. Integrated spectral power of intensity oscillations in individual structures in some frequency bands

Figure 6 illustrates distributions of the integrated spectral power calculated for the CaII K line over all spatial pixels of the region N05W00 studied. Blue and red colors indicate the integrated spectral power distributions at the K_1 and K_3 formation levels respectively. The black color shows the I_{K3} variation. It seems convenient to treat Figure 6, relying on frequency bands since the distribution is very complex, with power peaks distinct from the brightness peaks of the selected structures.

13

The 1.124–2.4 mHz frequency band (Figure 6, *a*). We have already noted a general increase in the oscillation power in the upper chromosphere for this band (see Figure 5). The maximum peak falls on one of the boundaries of plage "b03" ("fb5") at the K_1 and K_3 formation levels. Slightly lower peaks are observed in "fne1" and structures with intermediate brightness "x03" and "x04". At the K_3 level there is also a peak related to "x05" and "fx3". The power in "b01" and at its boundaries, despite exceeding the significance level of 0.95, is not high. It may be noted that the boundaries "fb2", "fn3", "fn4" and the boundaries "fne2" feature a decrease in power to a minimum in the lower level of the atmosphere near the temperature minimum. In "c01"–"c05", the power of low-frequency oscillations is generally low and reaches a minimum value in the structures "c02" and "c03" at both atmospheric levels considered.

The 2.4–4.0 mHz frequency band (Figure 6, *b*). In the so-called five-minute frequency band there is, in general, a decrease in the oscillation power with height and a complex distribution of power over the region considered. An exception is a spatial region $x\sim170"$–$180"$, where there is a slight excess of power at the upper level. Higher power peaks mainly occur at boundaries of the selected structures, except for "n02" in which peaks at two atmospheric levels coincide with the center of the structure. The most powerful peaks at the I_{K1} formation level occur in "fb2", "fb3", "fn3", "fn4", "c03", "n02", "fne2", and "x06". Sometimes they do not coincide with the peaks at the I_{K3} formation level, where a reduced oscillation power is observed instead of the peaks ("fn4", "x03", "c04", and "fne2").

The 4.0–5.2 mHz frequency band (Figure 6, *c*). In this band, the power at the I_{K3} level is also low compared to the I_{K1r} level. An exception is the vicinity of "c03", where there is a slight increase in the power of 4-minute oscillations at the upper level of the atmosphere. The highest peaks at both levels are located at boundaries, structures with intermediate brightness, and internetworks. The power in all identified plages is noticeably reduced.

The 5.2–6.8 mHz frequency band (Figure 6, *d*). In four of five "c" structures, the integrated spectral oscillation power is higher at the upper level of the atmosphere. Power peaks are observed not in the centers of the structures but at their boundaries. The highest power peak belongs to the boundary "fc1". In the structure "c02", which represents a slight increase in brightness next to "c01", there is the second-highest oscillation power peak, but it is higher at the I_{K1} formation level. Its maximum is at the boundary "fc2". There are also significant oscillation power peaks at both atmospheric levels in "x02" and "x03", "fx3" and "fc4", "fc7". The oscillation power drops noticeably in "b01", "n01", "b02", and "b03". However, in "n02" and especially at the boundary "fne2", the oscillation power is higher, especially in the lower level of the atmosphere.

The 8.0–16 mHz frequency band (Figure 6, *e*). In this rather wide band, the oscillation power is not very high, but in general it is higher at the I_{K3} level. Power peaks mainly occur at the boundaries of the structures. In "c01", "c04", and "c05", high-frequency oscillations in their centers are detectable. The highest power peak occurs in "ne1" and at its boundary; slightly lower peaks, in "n01", "fn1", and "fb3".
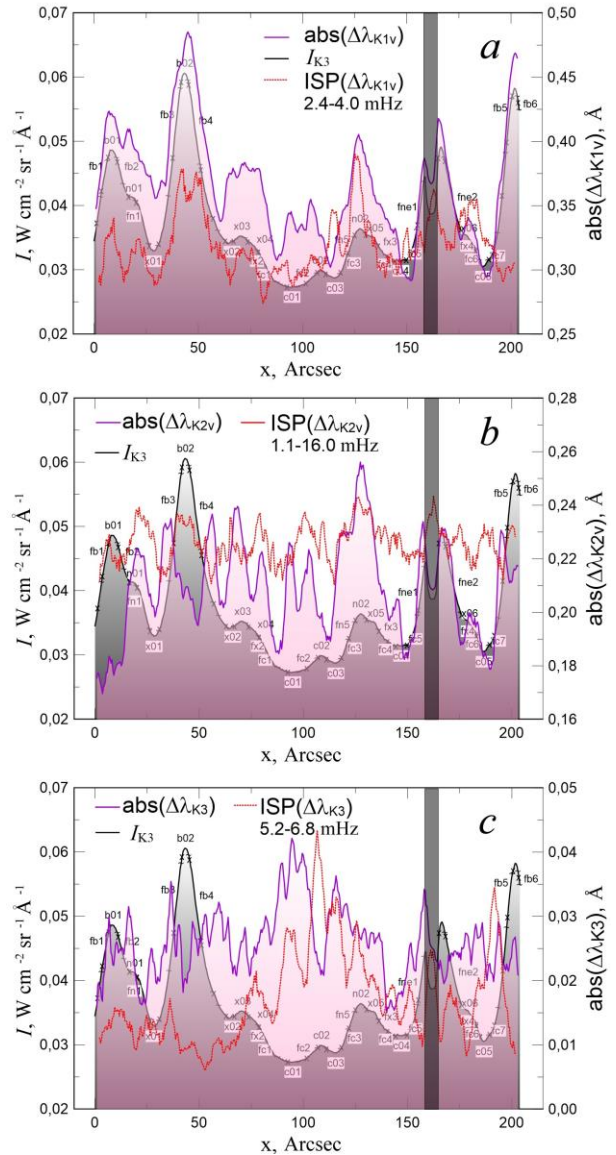

Figure 4. Time-averaged shifts of the CaII K line (purple curves and pink fill) at different formation levels of line parts: abs($\Delta\lambda_{K1v}$) (*a*); abs($\Delta\lambda_{K2v}$) (*b*); abs($\Delta\lambda_{K3}$) (*c*). The black curve and dark fill mark the spatial distribution of the time-averaged intensity I_{K3}. Red dashed curves indicate the spatial distribution of the integrated spectral power (ISP) of the corresponding parameter in one of the frequency bands. The other designations are the same as in Figure 2

The 1.124–16.0 mHz frequency band (Figure 6, *f*). In general, the oscillation power in the entire available frequency band is slightly lowered at the upper level. The maximum oscillation power at the lower atmospheric level is observed at the boundaries of "b01" and "b02". At the upper level, the highest power peaks are observed in "fc1", "c02", "c03", and "n02".

3. DISCUSSION

We have considered the spatial distribution of a number of the CaII K and 849.8 nm parameters and their temporal variations. The time-averaged spatial distributions of these parameters were also calculated, including intensities and shifts of calcium lines at different formation levels — K_1, X_0, K_2, and K_3. The distributions of
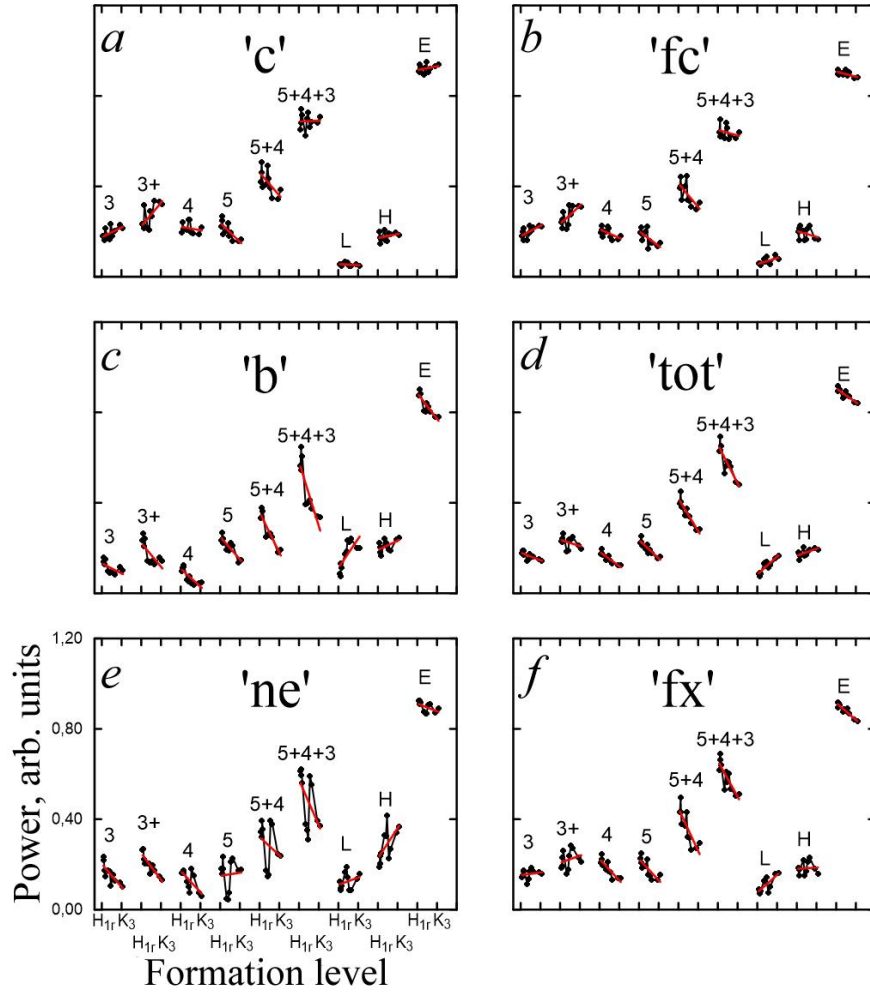
Figure 5. Variations of the spatially averaged integrated spectral power of intensity oscillations with height for some of the selected chromospheric structures and the entire region N05W00 (black curves). Interpolated values are highlighted in red. The following structures are shown: "internetwork" (*a*); "internetwork boundary" (*b*); "plage" (*c*); the entire region considered (*d*); "enhanced network" (*e*); "boundary of a region with intermediate brightness" (*f*). As height markers we took the heights of formation of I_{H1r}, I_{K1r}, I_{H1v}, I_{K1v}, I_{H2r}, I_{K2r}, I_{X0}, I_{H2v}, I_{K2v}, I_{H3}, I_{K3}. Designations along the X-axis show the first and the last of them. Numbers and letters mark the following frequency bands: "3" — 5.2–6.8 mHz; "3+" — 5.2–8.0 mHz; "4" — 4.4–5.2 mHz; "5" — 2.4–4.0 mHz; "5+4" — 2.4–5.2 mHz; "5+4+3" — 2.4–8.0 mHz; "L" — 1.124–2.4 mHz; "H" — 8.0–16.0 mHz; "E" — 1.124–16.0 mHz. The integrated spectral power along the Y-axis is given in arbitrary units

Table 1

Correlation between shifts $\Delta\lambda$, intensities I and oscillation power P

| №	Parameters	Region	Frequency, mHz	Correlation coefficient
1	abs($\Delta\lambda_{K1v}$)–I_{K1v}	0"–204"	–	0.95
2	abs($\Delta\lambda_{K2v}$)–I_{K2v}	0"–204"	–	0.13
3	abs($\Delta\lambda_{K3}$)–I_{K3}	0"–204"	–	–0.23
4	abs($\Delta\lambda_{K1v}$)–ISP($\Delta\lambda_{K1v}$)	0"–204"	2.4–4.0	0.32
		0"–100"	2.4–4.0	0.70
5	abs($\Delta\lambda_{K2v}$)–ISP($\Delta\lambda_{K2v}$)	0"–204"	1.1–16.0	0.28
6	abs($\Delta\lambda_{K3}$)–ISP($\Delta\lambda_{K3}$)	0"–204"	5.2–6.8	0.23
		0"–100"	5.2–6.8	0.45
7	abs($\Delta\lambda_{K1v}$)–P($\Delta\lambda_{K1v}$)	40"–49" (b02)	1.8	0.50
		91"–96" (c01)	6.5	0.51
8	abs($\Delta\lambda_{K2v}$)–P($\Delta\lambda_{K2v}$)	31"–37" (near b02)	2.1	0.55
		51"–58" (near b02)	12.4	0.61
		91"–96" (c01)	9.41	0.53
9	abs($\Delta\lambda_{K3}$)–P($\Delta\lambda_{K3}$)	31"–37" (near b02)	5.31	0.75
		91"–96" (c01)	2.33	0.63
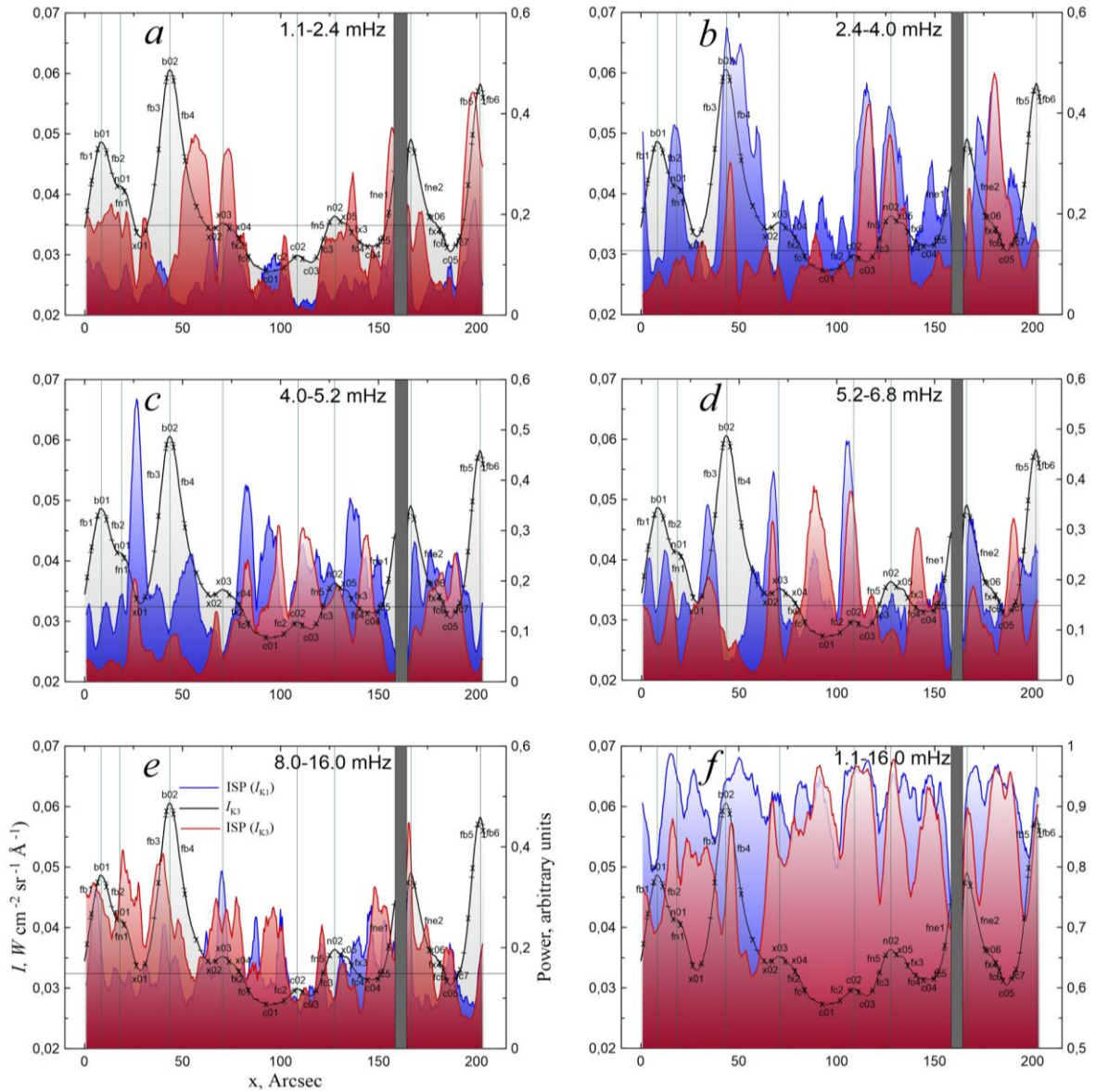
Figure 6. Distribution of integrated spectral power of intensity oscillations in the N05W00 region in the lower chromosphere (I_{K1r}, blue curve and fill) and in the upper chromosphere (I_{K3}, red curve and fill) in several frequency bands: low-frequency band (*a*); 5-minute band (*b*); 4-minute band (*c*); 3-minute band (*d*); high-frequency band (*d*); entire available frequency band (*e*). The black curve and gray fill indicate the I_{K3} distribution with the selected structures designated by numbers and letters. The black vertical stripe is a thread stretched across the spectrograph slit. Thin green vertical lines are centers of the main selected structures. The horizontal black line is a significance level of 0.95

shifts and intensities appeared to coincide in the lower chromosphere, whereas in the middle chromosphere the maximum line shifts occur not in the centers but at boundaries of bright magnetic structures (plages). This is consistent with the results obtained in [Heggland et al., 2011], in which numerical simulation of wave propagation in models of the solar atmosphere with different magnetic field configurations has been carried out. Heggland et al. [2011] note that all strong magnetic flux concentrations are associated with a region of high velocity amplitude higher up, and nearly all regions of high amplitude are connected with flux concentrations. Unlike the results of [Heggland et al., 2011], at the highest K_3 level we deal with, the highest shift amplitudes are observed in the quietest nonmagnetic structures of the region under study. One structure stands out

among them (see Figure 4, *c*, *x*=115 arcsec) with a slightly enhanced brightness, probably associated with a local increase in the magnetic flux. The line shift amplitudes ($\Delta\lambda_{K3}$) in this structure are much lower, with the highest power of velocity fluctuations in 5.2–8.0 mHz observed in it.

In the frequency band under study (1.124–16.0 mHz), peaks in the power spectrum (not shown) occur not at low frequencies, as might be expected for small-scale magnetic flux tubes (e.g., [Khomenko et al., 2008]), but at 5.5 and 7 mHz, which is also consistent with the results of [Heggland et al., 2011].

We have already mentioned that the line shifts are distributed over space more chaotically than intensities. The oscillatory power of $\Delta\lambda$ does not always correspond to the spatial distribution of shifts (see Figure 4). The

absence of a convincing correspondence between the oscillatory power of Δλ and the parameter itself makes it possible to suggest that a certain percentage of the line shifts is not periodic.

Let us take a closer look at our findings on the intensity oscillations in individual frequency bands.

Low-frequency intensity oscillations are detected at different levels of the solar atmosphere in different lines and solar features (see, e.g., [Damé et al., 1984; DeForest, Gurman, 1998; McAteer et al., 2003; Srivastava et al., 2008; Ozhogina, Teplitskaya, 2013, 2014]). Wave propagation with a frequency lower than the acoustic cutoff frequency of 5.2 mHz to the chromosphere [Bel, Leroy, 1977; Suematsu, 1990; De Pontieu et al., 2004; Jefferies et al., 2006] may be associated with a decrease in this frequency in network magnetic fields inclined with respect to the direction of gravity. This happens when the plasma β (the ratio of gas pressure to magnetic pressure) becomes <1. In accordance with these works, the increase in the power of low-frequency oscillations we have obtained occurs generally at the boundaries "f". Similar results from observations of intensity, magnetic field, and Doppler velocity oscillations in facular magnetic knots have been found in [Kobanov, Pulyaev, 2011; Chelpanov et al., 2015]. On the periphery of the knots, Chelpanov et al. [2015] detected oscillations in the range 1.5–3 mHz; and in the center of knots, in 3–6 mHz. The authors believe that this distribution of oscillations is due to the magnetic field topology — vertical in the center and inclined on the periphery. In most other structures, according to our data, the power of low-frequency oscillations is also increased in the middle chromosphere (Figure 6, *a*). Low-frequency oscillations occur in all regions — both in bright magnetic elements and in dark regions with a weak magnetic field (see also [Grigoryeva et al., 2016]).

The high-frequency band 8–16 mHz in our observations is much wider than the other selected bands, but its contribution to the oscillatory power is not very large. The greatest increase in the power of high-frequency oscillations in the middle chromosphere occurs at boundaries of bright structures, including two plages (Figure 6, *e*). The power of high-frequency oscillations also increases in a number of structures with low brightness. In general, the power of high-frequency oscillations in the region of interest is slightly increased in the upper chromosphere, and its distribution over structures is rather chaotic (Figure 6, *e*). Gafeira et al. [2017] from observations in the CaII H line have found high-frequency line intensity and width oscillations in slender fibrils. The answer to the question about the contribution of high-frequency waves to the solar atmosphere heating remains ambiguous. For example, Srivastava et al. [2021] note that at present the role of high-frequency waves in the energy balance of the solar atmosphere is underestimated. On the other hand, in many works devoted to the study of high-frequency oscillations, it is concluded that the energy of these oscillations is too low to maintain the temperature increase in the upper layers of the solar atmosphere, for example, [Carlsson et al., 2007; Fossum, Carlsson, 2006]. Further discussion of the conclusions drawn by Fossum, Carlsson [2005a, b,

2006] has shown that the results obtained by these authors are most likely associated with insufficient spatial resolution of TRACE (see, e.g., [Cuntz et al., 2007]). Cuntz et al. [2007] argue in favor of the fact that high-frequency acoustic waves (10–50 mHz) are sufficient to heat the nonmagnetic solar chromosphere. Bello Gonzalez et al. [2010] show that in the frequency band 5.2–10 mHz for an altitude of ~250 km the acoustic flux exceeds radiative losses. One-dimensional numerical simulation [Shoda, Yokoyama, 2018] has revealed that the high-frequency oscillations (20–25 mHz) observed in chromospheric spicules occur in the chromosphere due to conversion of longitudinal waves into transverse ones. The energy flux of these high-frequency waves is small; it is several times smaller than the total energy flux, so it is necessary to consider low-frequency and high-frequency waves at a time. High-frequency MHD waves (9–17 mHz) were also registered in small-scale structures from observations of brightness temperature fluctuations [Jafarzadeh et al., 2021].

In contrast to low-frequency and high-frequency oscillations, 5-minute oscillations, according to our findings, are attenuated in the upper chromosphere in most of the selected structures (see Figure 5). An exception is the enhanced network in which the integrated spectral oscillation power varies non-monotonically with height in almost all the frequency bands considered. We calculated the correlation coefficients of 5-minute oscillations in the upper photosphere and the upper chromosphere for the selected structures (not shown). Our results show that at these levels there is a high correlation between 5-minute oscillations in a quiet region outside a coronal hole (Figure 6, *b*). These results do not agree with the conclusions drawn by Chelpanov et al. [2021]; the authors did not detect general oscillations in the photosphere and chromosphere outside a coronal hole. From our observations and from the observations made by Kayshap et al. [2018] it follows that different structures of the region under study differently participate in propagation or non-propagation of 5-minute waves. In the conclusions drawn in [Kayshap et al., 2018], it is particularly noted that waves from the photosphere can propagate upwards to the transition region both as 3-minute waves and (in some locations) 5-minute ones. We believe that a larger number of observations are needed to get an unambiguous answer.

According to our findings, 5-minute oscillations occur not only in bright magnetic structures. For example, in two of three observed plages "b01" and "b03" (Figure 6, *b*), the power of 5-minute oscillations is low. The question about propagation of 5-minute oscillations in strong magnetic fields is extensively discussed in the literature. Thus, Centeno et al. [2006] show that 5-minute waves propagate from the photosphere to the chromosphere in a facular region. An example of such propagation may be our structures "ne1", "n02", and "b01" (Figure 6, *b*). Nevertheless, according to our data, the highest power of 5-minute oscillations in the middle chromosphere was not in bright magnetic structures but in structures with lower brightness. This is consistent with the conclusions drawn by Khomenko et al. [2008]

that 5-minute waves can also propagate into the chromosphere in almost vertical small-scale magnetic flux tubes in which the radiative relaxation time scale is sufficiently small. This also agrees with the results received in [Gupta et al., 2013], where 5-minute oscillations (2.76–4.02 mHz) are demonstrated to occur mainly in dark nonmagnetic regions. Interesting results have been obtained in [Rajaguru et al., 2019] — the authors observed wave propagation with a frequency 2–4.0 mHz in isolated almost vertical magnetic flux tubes, as well as a decrease in their amplitude with height. Propagation of these waves is associated with a decrease in the acoustic cutoff frequency due to a decrease in the radiative relaxation time. The wave damping with height is attributed to wave steeping and dissipation. The pattern of distribution of 5-minute waves seems in general to be rather complex. The ambiguity may be amplified by the interference of waves from close sources, analyzed in [Heggland et al, 2011], the authors simulated wave propagation in inclined and vertical magnetic fields.

Both 4-minute and 3-minute oscillations are attenuated in bright magnetic elements (such as "b01", "b02" in Figure 6, *c*, *d*).

An exception is the boundary of "ne1", where 3-minute oscillations are enhanced, especially in the lower chromosphere. In general, these oscillations occur in internetworks with maxima at their boundaries and are enhanced in these structures at the upper level. The power distribution in 3-minute and 4-minute bands is similar to that observed in [Lites et al., 1993; Gupta et al., 2013]. A similar pattern for the 3-minute band is supported by model calculations of wave propagation made in [Heggland et al., 2011], where the authors show that 3-minute waves dominate in regions with a weak magnetic field.

As already mentioned, our results have shown that the power in the 3-minute and 4-minute bands is higher in the upper chromosphere for the structures with a weak magnetic field (Figure 5, *a*, *b* and Figure 6, *c*, *d*). The power of 3-minute oscillations averaged over all structures decreases in the upper chromosphere compared to the upper photosphere, as does the power of 4-minute and 5-minute oscillations (see Figure 5, *d*). Four-minute oscillations are rarely considered separately in the literature. For instance, in the power spectra calculated by Deubner, Fleck [1990] there are peaks in this particular frequency band for both dark and bright elements of the chromospheric network. This frequency band was treated in particular by Kobanov [2000] who studied oscillations in the lower chromosphere. Peaks in the 4-minute frequency band are clearly visible in the power spectra obtained by Chelpanov et al. [2015]; the authors studied intensity, Doppler velocity, and magnetic field variations in the centers of solar faculae and on

their periphery. The power amplification at a frequency of 4 mHz has been found by Jafarzadeh et al. [2021] from datasets with the weakest magnetic fields.

The oscillation power decrease with height in our frequency band 2.4–8 mHz (see Figure 5) is similar to that obtained in [Mein, Schmieder, 1981] for a quiet region. These authors used observations in the CaII and MgI lines and the frequency band 2.5–8.3 mHz, which practically coincides with our band. They observed damping of the wave energy flux from the photosphere to the chromosphere (up to an altitude of 1500 km) by about an order of magnitude (Figure 3, *b* in the work of these authors).

To explore the possible relationship between oscillations in the same structures at different atmospheric levels, we have calculated correlation coefficients for different sets of selected parameters. A very inhomogeneous patten was found. There proved to be no correlation between oscillations in all frequency bands in a number of structures in three atmospheric levels (K_1, K_2, and K_3). In some structures there is a correlation of oscillations only between two of the three atmospheric levels, for example, between K_1 and K_2 or between K_2 and K_3. In order to figure out how and where the oscillations propagate, we plan to include the phase ratios, derived from the spectral analysis, in a follow-up study.

We have compared the oscillatory processes occurring in two regions of the quiet Sun, located at the base of a coronal hole, and one region outside the coronal hole. It turned out that in both the lower and upper chromosphere the intensity oscillation power is higher in the region outside the coronal hole in most frequency bands. An exception is the 4-minute frequency band, where this trend is weak or absent at both chromospheric levels. Table 2 lists the ratios of ISP of CaII K line intensity oscillations averaged over all spatial structures in different frequency bands for a region located outside the coronal hole to ISP in two regions located at the base of the coronal hole at the levels of the lower and upper chromosphere (K_1 and K_3).

Nevertheless, the behavior of the integrated spectral power of intensity oscillations with height differs little in three regions (see [Grigoryeva et al., 2016]). The results are presented in Figures 5, 6, and 13 in [Grigoryeva et al., 2016]. It can be seen that the main feature of the behavior of intensity oscillations with height is a decrease in their power in all frequency bands except the low-frequency one (1.124–2.4 mHz). The oscillation power also increases on average with height in the 3-minute band (5.2–6.8 mHz) in the structures with a weak magnetic field. In this context, we are interested in the result reported in [Abbasvand et al., 2020]. In nonmagnetic areas of the quiet region for the 854.2 nm CaII line formation height, the calculated acoustic flux fully

Table 2

Ratios $ISP_{N05W00}/ISP_{S25W12}$ and $ISP_{N05W00}/ISP_{S25W17}$

Level	$ISP_{N05W00}/ISP_{S25W12}$					$ISP_{N05W00}/ISP_{S25W17}$				
	3 min	4 min	5 min	L	E	3 min	4 min	5 min	L	E
K_1	1.47	1.37	1.28	1.29	1.43	1.48	1.07	1.20	1.27	1.32
K_3	1.85	1.42	1.28	1.25	1.54	1.44	0.93	1.20	1.58	1.34

compensates for radiative losses in the middle chromosphere 1000–1400 km. The main contributor of the power spectrum is 6–7 mHz frequencies. At the same time, at 1600–1900 km the acoustic flux contribution is insufficient to balance radiative losses; an additional power supplier is required in this case. Our results on the frequency bands 5.2–6.8 mHz, 5.2–8.0 mHz for the structures with a weak magnetic field (see Figure 5) show qualitative similarity with the result from [Abbasvand et al., 2020]. The integrated spectral power in these two bands has a nonmonotonic behavior, but becomes the highest in the lower chromosphere (1000–1300 km) and decreases as the K_3 formation level (~1750–1900 km) is approached. This trend for the structures with low and intermediate brightness is also traced in our work ([Grigoryeva et al., 2016], Figure 13), where we have examined two regions at the base of a coronal hole.

CONCLUSION

1. At the level of the lower chromosphere, the line shift distributions in plages coincide with the intensity distribution, whereas in the upper chromosphere the maximum line shifts occur not in central parts of plages but at their boundaries.

2. The integrated spectral power of Ca II line intensity oscillations in the entire frequency band 1.124–16 mHz, as well as in the 3-minute, 4-minute, and 5-minute bands decreases with height from the level of the lower chromosphere to the level of the upper chromosphere in almost all structures.

3. In the low-frequency band, the oscillation power from the lower chromosphere to the upper one increases in almost all structures.

4. In the 3-minute band, the oscillation power in the structures with a weak magnetic field becomes the highest in the lower chromosphere and decreases slightly in the upper chromosphere.

5. The integrated spectral oscillation power in the high-frequency band in most structures increases with height.

Comparing the results of the study of the quiet Sun's regions located at the base of a coronal hole and the region located outside a hole (this work) has shown that there are both similarities and differences in the manifestation of dynamic processes in the same frequency bands in regions with different magnetic field structures. Common trends are discussed in Subsections 2, 3, 4. The difference we observe is that the integrated spectral power of Ca II line intensity oscillations is generally higher in the region outside a coronal hole.

REFERENCES

Abbasvand V., Sobotka M., Švanda M., Heinzel P., García-Rivas M., Denker C., Balthasar H., et al. Observational study of chromospheric heating by acoustic waves. *Astron. Astrophys.* 2020, vol. 642, A52. DOI: 10.1051/0004-6361/202038559.

Athay R.G. Radiative energy loss from the solar chromosphere and corona. *Astrophys. J.* 1966, vol. 146, pp. 223–240.

Ballester J.L., Alexeev I., Collados M., Downes T., Pfaff R.F., Gilbert H., Khodachenko M., et al. Partially ionized plasmas in astrophysics. *Space Sci. Rev.* 2018, vol. 214, iss. 2, A58. DOI: 10.1007/s11214-018-0485-6.

Ballester J.L., Soler R., Terradas J., Carbonell M. Nonlinear coupling of Alfvén and slow magnetoacoustic waves in partially ionized solar plasmas. *Astron. Astrophys.* 2020, vol. 641, A48, 17 p.DOI: 10.1051/0004-6361/202038220.

Beck C., Schmidt W., Rezaei R., Rammacher W. The signature of chromospheric heating in CaII H spectra. *Astron. Astrophys.* 2008, vol. 479, pp. 213–227. DOI: 10.1051/0004-6361:20078410.

Beck C., Khomenko E., Rezaei R., Collados M. The energy of waves in the photosphere and lower chromospheres. I. Velocity statistics. *Astron. Astrophys.* 2009, vol. 507, pp. 453–467. DOI: 10.1051/0004-6361/200911851.

Bel N., Leroy B. Analytical study of magneto-acoustic gravity wave. *Astron. Astrophys.* 1977, vol. 55, pp. 239–243.

Bello González N., Flores Soriano M., Kneer F., Okunev O. On the energy flux in acoustic waves in the solar atmosphere. *Memorie della Societa Astronomica Italiana.* 2010, vol. 81, pp. 757–762.

Bjørgen J.P., Sukhorukov A.V., Leenaarts J., Carlsson M., de la Cruz Rodríguez J., Scharmer G.B., Hansteen V.H. Three-dimensional modeling of the CaII H and K lines in the solar atmosphere. *Astron. Astrophys.* 2018, vol. 611, A62. DOI: 10.1051/0004-6361/201731926.

Carlsson M. Chromospheric modeling. *ASP Conference Ser.* 2006, vol. 354, pp. 291–300.

Carlsson M., Hansteen V.H., De Pontieu B., McIntosh S., Tarbell T.D., Shine D., Tsuneta S., et al. Can high frequency acoustic waves heat the quiet Sun chromosphere? *Publ. Astron. Soc. Japan.* 2007, vol. 59, pp. S663–S668.

Centeno R., Collados M., Trujillo Bueno J. Oscillations and wave propagation in different solar magnetic features. *ASP Conference Ser.* 2006, vol. 358, pp. 465–470.

Chelpanov A.A., Kobanov N.I., Kolobov D.Yu. Characteristics of oscillations in magnetic knots of solar faculae.*Astronomy Rep.* 2015, vol. 59, no. 10, pp. 968–973. DOI: 10.1134/ S1063772915090036.

Chelpanov A., Kobanov N., Chelpanov M., Kiselev A. Propagating oscillations in the lower atmosphere under coronal holes. *Solar Phys.* 2021, vol. 296, iss. 12, article id. 179, 13 p. DOI: 10.1007/s11207-021-01909-y.

Cowling T.G. The dissipation of magnetic energy in an ionized gas. *MNRAS.* 1956, vol. 116, pp. 114–124.

Cuntz M., Rammacher W., Musielak Z.E. Acoustic heating of the solar chromosphere: present indeed and locally dominant. *Astrophys. J.* 2007, vol. 657, pp. L57–L60.

Damé L., Gouttebroze P., Malherbe J.-M. Observation and analysis of intensity oscillations in the solar K-line. *Astron. Astrophys.* 1984, vol. 130, pp. 331–340.

DeForest C.E., Gurman J.B. Observation of quasi-periodic compressive waves in solar polar plumes. *Astrophys. J.* 1998, vol. 501, pp. L217–L220.

De Pontieu B., Erdélyi R., James S.P. Solar chromospheric spicules from the leakage of photospheric oscillations and flows. *Nature.* 2004, vol. 430, pp. 536–539. DOI: 10.1038/nature02749.

Deubner F.-L., Fleck B. Dynamics of the solar atmosphere. III. Cell-network distinction of chromospheric oscillations. *Astron. Astrophys.* 1990, vol. 228, pp. 506–512.

Fossum A., Carlsson M. Response functions of the ultraviolet filters of *TRACE* and the detectability of high-frequency acoustic waves. *Astrophys. J.* 2005a, vol. 625, pp. 556–562.

Fossum A., Carlsson M. High-frecuency acoustic waves are not sufficient to heat the solar chromospheres. *Nature.* 2005b, vol. 435, pp. 919–921. DOI: 10.1038/nature03695.

Fossum A., Carlsson M. Determination of the acoustic wave flux in the lower solar chromospheres. *Astrophys. J.* 2006, vol. 645. pp. 579–592.

Gafeira R., Jafarzadeh S., Solanki S.K., Lagg A., van Noort M., Barthol P., Rodríguez J.B., et al. Oscillations on width and intensity of slender CaII H fibrils from SUNRISE/SuFI. *Astrophys J. Suppl. Ser.* 2017, vol. 229, article id. 7, 6 p. DOI: 10.3847/1538-4365/229/1/7.

Goodman M.L. On the mechanism of chromospheric network heating and the condition for its onset in the sun and other solar–type stars. *Astrophys. J.* 2000, vol. 533, pp. 501–522.

Grigoryeva S.A., Turova I.P., Ozhogina O.A. Studying Ca II line profile shapes and dynamic processes in the solar chromospheres at the base of a coronal hole. *Solar Phys.* 2016, vol. 291, pp. 1977–2002. DOI: 10.1007/s11207-016-0951-9.

Gupta G.R., Subramanian S., Banerjee D., Madjarska M.S., Doyle J.G. Nature of quiet Sun oscillations using data from the *Hinode*, TRACE, and SOHO spacecraft. *Solar Phys.* 2013, vol. 282, pp. 67–86. DOI: 10.1007/s11207-012-0146-y.

Heggland L., Hansteen V. H., De Pontieu B., Carlsson M. Wave propagation and jet formation in the chromospheres. *Astrophys. J.* 2011, vol. 743, article id. 142, 27 p. DOI: 10.1088/0004-637X/743/2/142.

Jafarzadeh S., Wedemeyer S., Fleck B., Stangalini M., Jess D.B., Morton R.J., Szydlarski M., et al. An overall view of temperature oscillations in the SOLAR chromosphere with ALMA. *Philosophical Transactions of the Royal Society A.* 2021, vol. 379, 28 p. DOI: 10.1098/rsta.2020.0174.

Jefferies S.M., McIntosh S.W., Armstrong J.D., Bogdan T.J., Cacciani A., Fleck B. Magnetoacoustic portals and the basal heating of the solar chromosphere. *Astrophys. J.* 2006, vol. 648, pp. L151–L155. DOI: 10.1086/508165.

Jess D.B., Morton R.J., Verth G., Fedun V., Grant S.D.T., Giagkiozis I. Multiwavelength studies of MHD waves in the solar chromosphere. An overview of recent results. *Space Sci. Rev.* 2015, vol. 190, pp. 103–161. DOI: 10.1007/s11214-015-0141-3.

Judge P.G. New perspectives on the photosphere/corona interface (Keynote). *ASP Conference Ser.* 2009, vol. 415, pp. 7–14.

Judge P.G. The chromosphere: gateway to the corona?... Or the purgatory of solar physics? *Memorie della Societa Astronomica Italiano.* 2010, vol. 81, pp. 543–552.

Judge P.G., Tarbell T.D., Wilhelm K. A study of chromospheric oscillations using the SOHO and TRACE spacecraft. *Astrophys. J.* 2001, vol. 554, pp. 424–444.

Kayshap P., Murawski K., Srivastava A.K., Musielak Z.E., Dwivedi B.N. Vertical propagation of acoustic waves in the solar internetwork as observed by IRIS. *MNRAS.* 2018, vol. 479, pp. 5512–5521. DOI: 10.1093/mnras/sty1861.

Khodachenko M.L., Arber T.D., Rucker H.O., Hanslmeier A. Collisional and viscous damping of MHD waves in partially ionized plasmas of the solar atmosphere. *Astron. Astrophys.* 2004, vol. 422, pp. 1073–1084. DOI: 10.1051/0004-6361:20034207.

Khomenko E., Collados M. Heating of the magnetized solar chromosphere by partial ionization effects. *Astrophys. J.* 2012, vol. 747, pp. 87–98. DOI: 10.1088/0004-637X/747/2/87.

Khomenko E., Santamaria I.C. Magnetohydrodynamic waves driven by p-modes. *J. Physics Conf. Ser.* 2013, vol. 440, iss. 1, article id. 012048.. DOI: 10.1088/1742-6596/440/1/012048.

Khomenko E., Centeno R., Collados M., Trujillo Bueno J. Channeling 5 minute photospheric oscillations into the solar outer atmosphere through small-scale vertical magnetic flux tubes. *Astrophys. J.* 2008, vol. 676, pp. L85–L88.

Kobanov N.I. Lower chromospheres oscillations near 4 mHz. *Astron. Astrophys. Trans.* 2000, vol. 19, iss. 2, pp. 103–113. DOI: 1080/10556790008241354.

Kobanov N.I., Pulyaev V.A. Spatial distribution of oscillations in faculae. *Solar Phys.* 2011, vol. 268, pp. 329–334. DOI: 10.1007/s11207-010-9581-9.

Kopecký, M., Kuklin, G.V. Concerning the 11-year variation of average lifetime of sunspot groups. *Issledovanija po geomagnetizmu, aeronomii i fizike Solntsa* [Research on Geomagnetism, Aeronomy and Solar Physics]. 1971, iss. 2, pp. 167–179. (In Russian).

Leenaarts J., de la Cruz Rodríguez J., Danilovic S., Scharmer G., Carlsson M. Chromospheric heating during flux emergence in the solar atmosphere. *Astron. Astrophys.* 2018, vol. 612, A28. DOI: 10.1051/0004-6361/201732027.

Lites B.W., Rutten R.J., Kalkofen W. Dynamics of the solar chromosphere. I. Long-period network oscillations. *Astrophys. J.* 1993, vol. 414, pp. 345–356.

Martinez-Sykora J., De Pontieu B., Hansteen V., Carlsson M. The role of partial ionization effects in the chromosphere. *Philosophical Transactions of the Royal Society A.* 2015, vol. 373, iss. 2042, pp. 20140268–20140268. DOI: 10.1098/rsta.2014.0268.

McAteer R.T.J., Gallagher P.T., Williams D.R., Mathioudakis M., Bloomfield D.S., Phillips K.J.H., Keenan F.P. Observational evidence for mode coupling in the chromospheric network. *Astrophys. J.* 2003, vol. 587, pp. 806–817.

Mein N., Schmieder B. Mechanical flux in the solar chromospheres. III. Variation of the mechanical flux. *Astron. Astrophys.* 1981, vol. 97, pp. 310–316.

Molnar M.E., Reardon K.P., Cranmer S.R, Kowalski A.F., Chai Y., Gary D. High-frequency wave power observed in the solar chromosphere with IBIS and ALMA. *Astrophys. J.* 2021, vol. 920, article id. 125, 21 p. DOI: 10.3847/1538-4357/ac1515.

Ozhogina O.A., Teplitskaya R.B. Center-to-limb variation of CaII line brightness oscillations in the solar chromosphere. *Astronomy Lett.* 2013, vol. 39, no. 4, pp. 279–289. DOI: 10.1134/S1063773713030031.

Ozhogina O.A., Teplitskaya R.B. Center-to-limb variation of low-frequency CaII line brightness oscillations in the solar chromosphere. *Astronomy Lett.* 2014, vol. 40, no. 6, pp. 361–371. DOI: 10.1134/S1063773714060061.

Piddington J.H. Solar atmospheric heating by hydromagnetic waves. *MNRAS.* 1956, vol. 116, pp. 314–323.

Pietarila A., Socas-Navarro H., Bogdan T., Carlsson M., Stein R.F. Simulation of quiet-Sun waves in the CaII infrared triplet. *Astrophys. J.* 2006, vol. 640, pp. 1142–1152.

Rajaguru S.P., Sangeetha C.R., Tripathi D. Magnetic fields and the supply of low-frequency acoustic wave energy to the solar chromospheres. *Astrophys. J.* 2019, vol. 871, article id. 155, 15 p. DOI: 10.3847/1538-4357/aaf883.

Reardon K.P. The effects of atmospheric dispersion on high-resolution solar spectroscopy. *Solar Phys.* 2006, vol. 239, pp. 503–517. DOI: 10.1007/s11207-006-0283-2.

Reardon K.P., Uitenbroek H., Cauzzi G. The solar chromospheres at high resolution with IBIS. III. Comparison of CaII K and CaII 854.2 nm imaging. *Astron. Astrophys.* 2009, vol. 500, pp. 1239–1247. DOI: 10.1051/0004-6361/200811223.

Shibata K., Nakamura T., Matsumoto T., Otsuji K., Okamoto T.J., Nishizuka N., Kawate T., et al. Chromospheric anemone jets as evidence of ubiquitous reconnection. *Science.* 2007, vol. 318, pp. 1591–1594. DOI: 10.1126/science.1146708.

Shine R.A., Linsky J.L. Physical properties of solar chromospheric plages. II: Chromospheric plage models. *Solar Phys.* 1974, vol. 39, pp. 49–77.

Shoda M., Yokoyama T. High-frequency spicule oscillations generated via mode conversion. *Astrophys. J.* 2018, vol. 854, article id. 9, 10 p. DOI: 10.3847/1538-4357/aaa54f.

Simon G.W. A practical solution of the atmospheric dispersion problem. *Astronom. J.* 1966, vol. 71, no. 3, pp. 190–194.

Smith P.D., Sakai J.I. Chromospheric magnetic reconnection: two-fluid simulations of coalescing current loops. *Astron. Astrophys*. 2008, vol. 486, pp. 569–575. DOI: 10.1051/0004-6361:200809624.

Srivastava A.K., Kuridze D., Zaqarashvili T.V., Dwivedi B.N. Intensity oscillations observed with Hinode near the south pole of the Sun: leakage of low frequency magneto-acoustic waves into the solar corona. *Astron. Astrophys*. 2008, vol. 481, pp. L95–L98. DOI: 10.1051/0004-6361:20079328.

Srivastava A.K., Ballester J. L., Cally P.S., Carlsson M., Goossens M., Jess D.B., Khomenko E., et al. Chromospheric heating by magenohydrodynamic waves and instabilities. *JGR Space Phys*. 2021, vol. 126, e2020JA029097. DOI: 10.1029/2020JA029097.

Suematsu Y. Influence of photospheric 5-minute oscillations on the formation of chromospheric fine structures. *Progress of Seismology of the Sun* and Stars. *Lecture Notes in Physics.* Berlin, Heidelberg. Springer. 1990, vol. 367, pp. 211–214. DOI: 10.1007/3-540-53091-6_83.

Taroyan Y., Erdelyi R. Heating diagnostics with MHD waves. *Space Sci. Rev*. 2009, vol. 149, pp. 229–254. DOI: 10.1007/s11214-009-9506-9.

Teplitskaya R.B., Turova I.P., Kuklin G.V. The study of the dynamic process of umbral flashes. *Publ. Debrecen Heliophysical Obs*. 1983, vol. 5, pp. 267–284.

Teplitskaya R.B., Ozhogina O.A., Turova I.P. Brightness distribution at the base of a coronal hole. *Astron. Lett*. 2006, vol. 32, no. 2, pp. 120–127. DOI: 10.1134/S106377370602006X.

Teplitskaya R.B., Turova I.P., Ozhogina O.A. Intensity oscillations at the feet of coronal holes. *Astronomy Lett*. 2009, vol. 35, no. 10, pp. 712–722.

Turova I.P. On the unusual Hε emission in a sunspot umbra spectrum. *Solar Phys*. 1994, vol. 150, pp. 71–79.

Turova I.P., Teplitskaya R.B., Kuklin G.V. The study of umbral flashes in the umbrae of two sunspots. *Solar Phys*. 1983, vol. 87, pp. 7–22. DOI: 10.1007/BF00151155.

Turova I.P., Grigoryeva S.A., Ozhogina O.A. Spatial and temporal variations of K CaII line profile shapes in different structures of the solar chromosphere. II. Determination technique and correlation relationships between the K CaII line parameters for K_1 and K_2 features. *Solar-Terrestrial Physics.* 2020. Vol. 6. Iss. 4. P. 10–16. DOI: 10.12737/stp-64202002.

Vernazza J.E., Avrett E.H., Loeser R. Structure of the solar chromosphere. III. Models of the EUV brightness components of the quiet sun. *Astrophys. J. Suppl. Ser*. 1981, vol. 45, pp. 635–725. DOI: 10.1086/190731.

von Uexküll M., Kneer F. Oscillations of the Sun's chromospheres. VII. K grains revisited. *Astron. Astrophys*. 1995, vol. 294, pp. 252–259.

Withbroe G.L., Noyes R.W. Mass and energy flow in the solar chromosphere and corona. *Ann. Rev. Astron. Astrophys.* 1977, vol. 15, pp. 363–387. DOI: 10.1146/annurev.aa.15.090177. 002051.

Zaqarashvili T.V., Khodachenko M.L., Rucker H.O. Magnetohydrodynamic waves in solar partially ionized plasmas: two-fluid approach. *Astron. Astrophys*. 2011, vol. 529, A82. DOI: 10.1051/0004-6361/201016326.

Zweibel E. G. Magnetic reconnection in partially ionized gases. *Astrophys. J*. 1989, vol. 340, pp. 550–557.

URL: https://SolarMonitor.org (accessed February 22, 2023).

How to cite this article